



ARTICLE

DOI: 10.1038/s41467-018-03472-w

OPEN

Amplification of heat extremes by plant CO₂ physiological forcing

Christopher B. Skinner¹, Christopher J. Poulsen ¹ & Justin S. Mankin ^{2,3,4}

Plants influence extreme heat events by regulating land-atmosphere water and energy exchanges. The contribution of plants to changes in future heat extremes will depend on the responses of vegetation growth and physiology to the direct and indirect effects of elevated CO₂. Here we use a suite of earth system models to disentangle the radiative versus vegetation effects of elevated CO₂ on heat wave characteristics. Vegetation responses to a quadrupling of CO₂ increase summer heat wave occurrence by 20 days or more—30–50% of the radiative response alone—across tropical and mid-to-high latitude forests. These increases are caused by CO₂ physiological forcing, which diminishes transpiration and its associated cooling effect, and reduces clouds and precipitation. In contrast to recent suggestions, our results indicate CO₂-driven vegetation changes enhance future heat wave frequency and intensity in most vegetated regions despite transpiration-driven soil moisture savings and increases in aboveground biomass from CO₂ fertilization.

¹Department of Earth and Environmental Sciences, University of Michigan, 1100 North University Ave, Ann Arbor, MI 48104, USA. ²Ocean and Climate Physics, Lamont-Doherty Earth Observatory, 61 Route 9W, P.O Box 1000, Palisades, NY 10964, USA. ³NASA Goddard Institute for Space Studies, New York, NY 10025, USA. ⁴Department of Geography, Dartmouth College, Hanover, NH 03755, USA. Correspondence and requests for materials should be addressed to C.B.S. (email: chrisbs@umich.edu)

Prolonged exposure to extreme heat, such as during a heat wave, imposes severe stresses on natural and human systems. Acute heat-related impacts include increased human morbidity and mortality^{1,2}, loss of livestock and crop failure³, increased wildfires⁴, and reductions in vegetation gross primary productivity (GPP)⁵. Heat wave frequency has recently increased over many parts of the globe, highlighting the exceptional sensitivity of heat extremes to even small changes in mean global warming^{6,7}. Given continued anthropogenic emissions of CO₂, climate models project further increases in heat wave occurrence, intensity, and duration, spurring a considerable effort to diagnose the processes that shape these events in current and future climates^{8–10}. Recent work has called attention to the potentially substantial, but largely unexplored and uncertain impact of CO₂-vegetation interactions, including CO₂ physiological forcing and CO₂ fertilization, on future heat wave characteristics^{11,12}. Here, we analyze a suite of Earth system models (ESMs) from the Coupled Model Intercomparison Project Phase 5 (CMIP5)¹³ in a set of idealized experiments to quantify the contribution of the vegetation response to CO₂ to projected heat wave changes and to better understand its role in shaping regional-scale and inter-model differences in projected future heat extremes.

In addition to serving as a greenhouse gas, CO₂ indirectly influences climate through its impact on vegetation growth and physiology. Under high CO₂, plant photosynthetic carbon fixation rates increase, while stomatal aperture is reduced or maintained¹⁴. The increase in photosynthesis and subsequent enhanced biomass production due to the non-radiative effects of higher CO₂ is known as CO₂ fertilization^{15,16}. The closing of stomata and subsequent reduction in stomatal conductance and transpiration (evaporation of water from the leaf interior) due to the non-radiative effects of higher CO₂ is known as CO₂ physiological forcing^{17,18}. While the magnitudes of the fertilization and physiological responses vary by plant species and under different environmental conditions, including water, light, and nutrient availability, observational and modeling evidence suggests that the two effects have opposing influences on climate^{19,20}. Though enhanced CO₂ often has a limited impact on leaf area index (LAI, defined as one-sided leaf area per unit ground surface area), in nutrient-limited regions, and in mature forests²¹, CO₂ fertilization can lead to enhanced LAI during the early stages of plant development^{21,22} and in regions that are water-limited²³. Greater LAI can enhance plant transpiration and surface evaporative cooling given sufficient moisture supply^{24,25}. Meanwhile, in regions that are not severely water-limited, CO₂ physiological forcing limits transpiration and enhances the ratio of sensible to latent heat fluxes at the leaf surface, increasing boundary layer temperatures^{17,26,27}.

Future changes in evapotranspiration (ET, the sum of transpiration and soil and canopy evaporation) have the potential to alter the characteristics of extreme heat events, such as heat waves. Heat waves are initiated when large-scale anticyclonic atmospheric patterns become stagnant^{7,28}. The severity of heat waves is amplified through feedbacks with the underlying land surface. Dry soils and low ET enhance surface sensible heating of the atmosphere and promote higher near-surface temperatures during the heat wave²⁹.

Given the impact of CO₂ physiological forcing and CO₂ fertilization (hereafter collectively referred to as CO₂ vegetation forcing) on surface moisture and energy fluxes, each may contribute to projected changes in future heat wave events, but the net effects on projected heat waves remain unresolved. The vegetation response to elevated CO₂ could mitigate the frequency and intensity of summer heat waves by increasing the springtime canopy water use efficiency (WUE) via CO₂ physiological forcing, thus increasing the soil water available for evapotranspirative cooling later in the peak of summer^{12,30,31}. For example, observed growing season water savings from CO₂-induced transpiration reductions range from up to ~2.15 mm day⁻¹ in some grassland ecosystems (exposed to 100% increase in CO₂)³⁰, to ~0.6 mm day⁻¹ in some temperate deciduous tree species (exposed to 40% increase in CO₂)²². Coupled with increasing summertime LAI via CO₂ fertilization, regions with greater soil moisture, particularly those that would have otherwise become water-limited during the summer, could see increases in transpiration, and, therefore, surface cooling when transpiration demand is high (such as during dry, hot days)¹². Indeed, observational and modeling work shows that irrigated cropland has experienced fewer summer hot extremes in recent decades as a result of enhanced ET from greater soil moisture^{32,33}. On the other hand, reduced stomatal conductance from CO₂ physiological forcing during the summer could diminish transpiration and the associated evaporative cooling in spite of increased LAI and soil moisture, elevating summer temperatures^{34,35}, allowing heat waves to increase in frequency, intensity, and length.

Most analyses of future heat extremes come from climate model simulations in which only the CO₂ radiative forcing is included, or from simulations in which CO₂ radiative forcing, CO₂ physiological forcing, and CO₂ fertilization are included simultaneously (e.g., ref.³⁶). Furthermore, previous work on CO₂ vegetation forcing focuses primarily on the mean temperature response, whether at seasonal or annual time scales, leaving the possibility that projected future CO₂ vegetation forcing influences the warm extremes of the daily temperature distribution differently than the mean of the distribution. Here we analyze a suite of ESMs from CMIP5 that include active biogeophysics and biogeochemistry to study the impact of CO₂ vegetation forcing (via a quadrupling of CO₂ concentrations) on four indices of heat extremes. Our results indicate that the vegetation response to elevated CO₂, primarily through reduced stomatal conductance and the hydrologic responses it induces, exacerbates CO₂ radiative-driven increases in extreme heat frequency and intensity.

Results

LAI and transpiration responses to CO₂ vegetation forcing.

Elevated CO₂ concentrations increase mean summer LAI via CO₂ vegetation forcing (see Methods and Tables 1–2) in each of the six CMIP5 models (see Supplementary Table 1) across all latitudes (JJAS in the Northern Hemisphere, DJFM in the Southern Hemisphere) (Fig. 1a, c, e, g). The stimulation of LAI by increasing CO₂ ($\Delta\text{LAI}/\Delta\text{CO}_2$ ppm) is greatest at relatively low CO₂ concentrations (Supplementary Table 2). LAI stimulation diminishes at higher CO₂ levels, indicating a trend towards LAI

Table 1 CMIP5 simulation names and associated CO₂ forcing

Simulation name	CO ₂ radiative forcing	CO ₂ physiological forcing	CO ₂ fertilization
TotalCO2 (1pctCO2)	Yes CO ₂ increases from 284 to 1132 ppm	Yes CO ₂ increases from 284 to 1132 ppm	Yes CO ₂ increases from 284 to 1132 ppm
RadCO2 (esmFdbk1)	Yes CO ₂ increases from 284 to 1132 ppm	No CO ₂ fixed at 284 ppm	No CO ₂ fixed at 284 ppm
VegCO2 (esmFixClim1)	No CO ₂ fixed at 284 ppm	Yes CO ₂ increases from 284 to 1132 ppm	Yes CO ₂ increases from 284 to 1132 ppm

Table 2 CO₂ forcing experiments

CO ₂ forcing type	Calculated as difference between	Reference climate for heat wave definition	Displayed in figures
CO ₂ vegetation forcing (avg CO ₂ 984 ppm)	Years 111–140 of <i>TotalCO2</i> minus Years 111–140 of <i>RadCO2</i>	Years 111–140 of <i>RadCO2</i>	Figures: 1,2,3,4,5; Supp. Figures: 1,2,3,4,5,6,7,9
CO ₂ radiative forcing (avg CO ₂ 984 ppm)	Years 111–140 of <i>TotalCO2</i> minus Years 111–140 of <i>VegCO2</i>	Years 111–140 of <i>VegCO2</i>	Figures: 4; Supp. Figures: 6,7
CO ₂ vegetation forcing (avg CO ₂ 575 ppm)	Years 58–87 of <i>TotalCO2</i> minus Years 58–87 of <i>RadCO2</i>	Years 58–87 of <i>RadCO2</i>	Supp. Figure: 8
CO ₂ vegetation forcing (avg CO ₂ 984 ppm)	Years 111–140 of <i>VegCO2</i> minus Years 1–29 of <i>VegCO2</i>	Years 1–29 of <i>VegCO2</i>	Supp. Figure: 8
CO ₂ radiative forcing (avg CO ₂ 984 ppm)	Years 111–140 of <i>RadCO2</i> minus Years 1–29 of <i>RadCO2</i>	Years 1–29 of <i>RadCO2</i>	Supp. Figure: 8
Total CO ₂ forcing (avg CO ₂ 984 ppm)	Years 111–140 of <i>TotalCO2</i> minus Years 1–29 of <i>TotalCO2</i>	Years 1–29 of <i>TotalCO2</i>	Figure: 4

saturation throughout the tropics, subtropics, and extratropics at the highest CO₂ concentrations (Fig. 1a, c, e). The largest changes in the magnitude of LAI from end-of-21st-century CO₂ vegetation forcing (average CO₂ ~984 ppm) are located in forested regions of the tropics and mid-latitudes where summer season LAI is high in the reference (baseline) climate period (Fig. 1g and Supplementary Fig. 2a–l). An evaluation of LAI in each model is provided in the Supplementary Information (Supplementary Note 1 and Supplementary Fig. 1) and in ref.³⁷.

Despite widespread LAI enhancement, average summer transpiration goes down in response to CO₂ vegetation forcing (Fig. 1b, d, f, h). In the tropics, the average rate of transpiration change over the course of CO₂ doubling ($\Delta\text{Tran}/\Delta\text{CO}_2$ ppm) levels off very slightly from the first CO₂ doubling (~284 ppm to 568 ppm) to the second CO₂ doubling (~568 ppm to 1132 ppm) in most models (note, ET is used for HadGEM2-ES) (Fig. 1b and Supplementary Table 2). In the subtropics and extratropics, CO₂ vegetation forcing initially enhances mean summer transpiration in a few models as increases in LAI potentially outpace reductions in stomatal conductance (though other climate system processes such as changes in rainfall may also contribute to the change) (Fig. 1d, f and Supplementary Table 2). However, most models exhibit reductions in transpiration throughout the 140-year simulations, and all models exhibit transpiration reductions over the course of the second doubling of CO₂ in the tropics, subtropics, and extratropics (Fig. 1b, d, f, and Supplementary Table 2). Transpiration reductions are concentrated in forested regions of the tropics and the Northern Hemisphere mid-to-high latitudes (Fig. 1h). Most models exhibit statistically significant reductions in transpiration in tropical Africa, Southeast Asia, and tropical South America, as well as throughout forested regions of mid-latitude North America, Europe, and Asia (Fig. 1h and Supplementary Fig. 2s–x). These regions correspond to the locations of climatologically high summer canopy density and transpiration in the reference climate period (Supplementary Fig. 2a–f and 2m–r). The results highlight the role of reduced stomatal conductance in shaping projected transpiration change.

CO₂ vegetation forcing simultaneously increases summer LAI and reduces summer transpiration over most of Earth's land surface (Fig. 2a). Across the models, between 58.4% (BCC-CSM1-1) and 86.7% (CESM1-BGC) of land area exhibits both positive LAI changes and negative transpiration changes (Fig. 2a). Increases in summer season transpiration due to CO₂ vegetation forcing are primarily confined to grassland and steppe regions in semi-arid portions of North America, Asia, Africa, and Australia, covering between 9.4% (CESM1-BGC) and 37.62% (BCC-CSM1-1) of total land area in the models (Fig. 2a and Supplementary Figure 2s–x). These regions of increasing summer transpiration exhibit relatively low summer LAI in the reference climate

simulations (Supplementary Fig. 2a–f) coupled with large percentage increases in LAI in response to CO₂ vegetation forcing (Supplementary Fig. 3a–f). This reveals that, in general, unless LAI increases substantially, a vegetated grid cell will exhibit reduced transpiration in response to future CO₂ vegetation forcing from high CO₂. Summer season WUE, defined as the ratio of summer GPP to summer transpiration, increases across all biomes (Supplementary Fig. 3g–l). The percent change in WUE is particularly large in the relatively warm semi-arid regions that exhibit mean increases in transpiration in response to CO₂ vegetation forcing (Supplementary Fig. 3g–l). This result highlights the important point that increases in WUE do not necessarily imply a reduction in total plant water use if photosynthesis and biomass increase³⁸.

Though most ESMs underestimate the global ratio of transpiration to total ET (Fig. 2b)³⁹, the reductions in transpiration from CO₂ vegetation forcing in the models, which, globally-averaged range from -7.5 mm summer⁻¹ in BCC-CSM1-1 to -29.5 mm summer⁻¹ in CESM1-BGC, are large enough to drive statistically significant summer ET declines in most forested regions (Supplementary Fig. 4a–f). As indicated by the decrease in evaporative fraction (the ratio of latent heat fluxes to the sum of latent and sensible heat fluxes), sensible heat fluxes increase at the expense of latent heat fluxes (and thus evaporative cooling) throughout the tropics and in regions of dense tree cover in the mid and high latitudes (Fig. 3a and Supplementary Fig. 4g–l). Enhanced boundary layer turbulence from greater sensible heat fluxes combined with reduced moisture fluxes from the surface reduces cloud formation and rainfall in many mid-to-high latitude locations, enhancing surface solar insolation (Supplementary Fig. 4m–x). In general, the greatest summer near-surface warming (daily maximum temperature) occurs in the mid and high latitudes where the evaporative fraction, cloud cover, and rainfall decrease (Fig. 3a, and Supplementary Figs. 4g–x and 5a–f). Increases in mean daily maximum tropical temperatures are slightly smaller despite large reductions in transpiration because cloud cover and rainfall change very little or even increase in some areas in response to CO₂ vegetation forcing (Supplementary Figs. 4m–x and 5a–f)³⁵.

Vegetation-driven temperature and heat extreme changes.

Mean maximum summer daily temperatures increase by more than 2 °C in response to CO₂ vegetation forcing throughout much of the Northern Hemisphere mid-to-high latitudes (Supplementary Fig. 5a–f). In tropical forests, most models project between 1 °C and 2 °C of warming (Supplementary Fig. 5a–f). With the exception of small areas in the subtropics and East Africa in CanESM2 and MPI-ESM-LR and a portion of the western

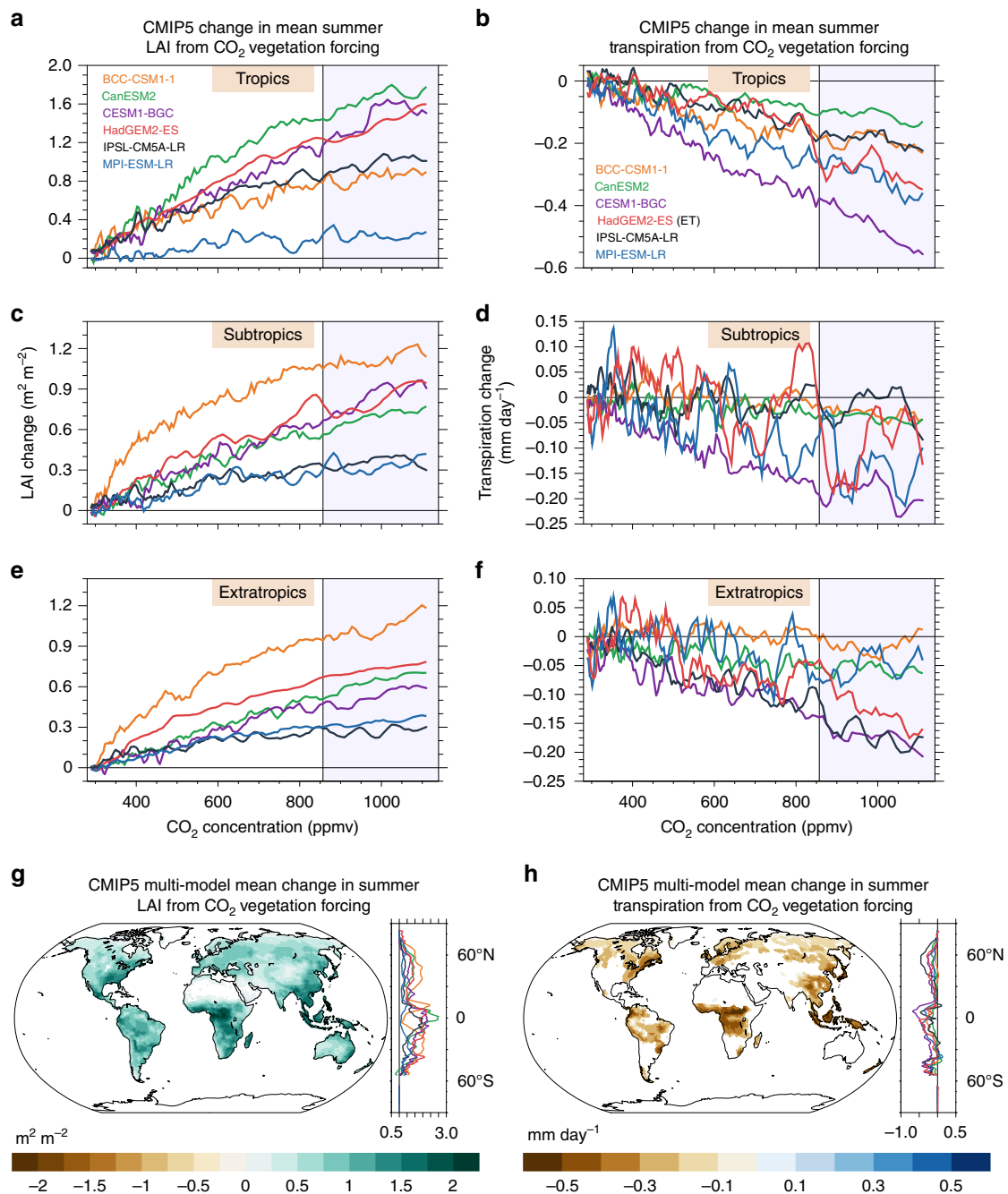


Fig. 1 Change in leaf area index and transpiration from CO₂ vegetation forcing. Change in mean summer **a, c, e** leaf area index (LAI) and **b, d, f** transpiration from CO₂ vegetation forcing. For each CO₂ concentration, the area-weighted value for the **a–b** tropics (15°S–15°N), **c–d** subtropics (15°S/N–30°S/N), and **e–f** extratropics (30°S/N–70°S/N) is calculated for the *TotalCO2* and *RadCO2* simulations. Then, the values are smoothed with a five-year running mean and the difference (*TotalCO2* – *RadCO2*) for each model is plotted. Multi-model mean change in summer **g** LAI and **h** transpiration from CO₂ vegetation forcing averaged over the final 30 years of the simulations (shaded region in **a–f**). Only statistically significant changes are plotted (Methods). Zonal averages of LAI and transpiration change (land grid points) for each model are plotted to right of each map. June–September (December–March) values are used in the Northern (Southern) Hemisphere. Evapotranspiration (ET) is used for HadGEM2-ES in **b, d, f**

Amazon in IPSL-CM5A-LR, no models exhibit statistically significant summer cooling due to CO₂ vegetation forcing (Supplementary Fig. 5a–f). Given that transpiration occurs primarily during daylight hours, CO₂ physiological forcing acts preferentially on daily maximum temperature, increasing the diurnal temperature range over vegetated regions (Supplementary Fig. 5g–l), though it should be noted that models do not accurately simulate nocturnal stomatal conductance⁴⁰.

CO₂ vegetation forcing also enhances the intensity of the hottest summer season days (Fig. 3b). The hottest daily maximum temperature experienced during the summer increases by ~2.5 °C across the Northern Hemisphere high latitudes, and by up to 2 °C across portions of the Amazon, Congo, and Southeast Asia. In some models, for example, CESM1-BGC and HadGEM2-ES, warming of the maximum daily summer temperature exceeds 3 °C over broad stretches of the tropics and the Northern Hemisphere mid and high latitudes (Supplementary Fig. 5m–r).

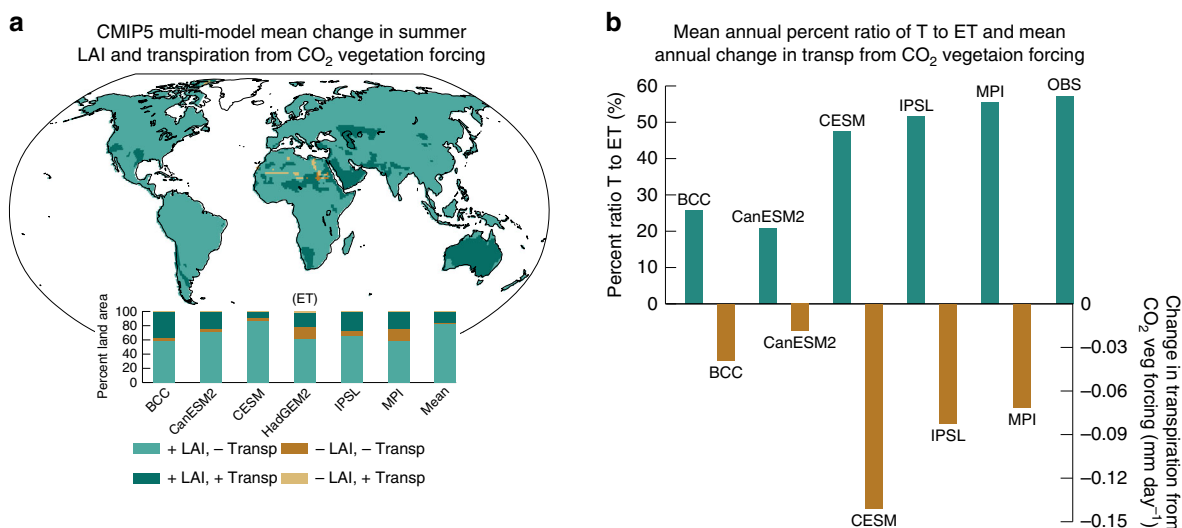


Fig. 2 Changes in leaf area index and transpiration from CO₂ vegetation forcing. **a** Map of summer leaf area index (LAI) and transpiration changes of a particular direction for the CMIP5 multi-model mean. Bar plots of the percentage of land area with LAI and transpiration changes of a particular direction. **b** (top) Global mean annual percent ratio of transpiration to evapotranspiration (T to ET) from the CMIP5 models and from observations provided in Wei et al. (2017). **b** (bottom) Global mean annual change in transpiration in the CMIP5 models from CO₂ vegetation forcing. The values for the ratio of T to ET come from years 18–34 (CO₂ ~ 340–398 ppm) in each model's *TotalCO2* simulation. Years 18–34 are chosen to closely match the CO₂ values during the years 1982–2014, which are used in Wei et al. (2017). Area-weighted averages are calculated from 60°S–90°N and do not include Greenland. June–September (December–March) values are used in the Northern (Southern) Hemisphere. Evapotranspiration (ET) is used for HadGEM2-ES

The boundary layer and surface water and energy flux changes from CO₂ vegetation forcing alter heat wave characteristics across most vegetated areas of the globe. Models exhibit robust increases in total heat wave days (HWTd) each summer (Fig. 4a and Supplementary Fig. 6a–f). Similar to the pattern of mean warming, heat wave days increase most over forested areas of the mid-to-high latitudes and tropics. On average, large portions of North America, Europe, Asia, and the La Plata basin of South America experience between 15 and 25 more heat wave days each summer from CO₂ vegetation forcing. In the tropics, warming from CO₂ vegetation forcing leads to increases in excess of 30 heat wave days per summer season. In comparison to the pattern of heat wave day changes from CO₂ radiative forcing (see Methods, and Supplementary Fig. 6a–l), CO₂ vegetation forcing primarily impacts wetter, vegetated areas of the mid and high latitudes (Fig. 4a). In the Northern Hemisphere mid-to-high latitudes, heat wave day increases from CO₂ vegetation forcing are roughly 30 to 50% of the CO₂ radiative-driven response (Fig. 4e).

Note that the zonal average change in heat wave days from the total CO₂ forcing (see Methods) is plotted for illustrative purposes only (Fig. 4a). Given the choice of different reference climate for the heat wave definitions (see Methods), and because the radiative and vegetation forcings are not independent, the individual changes in heat wave characteristics from CO₂ vegetation forcing and CO₂ radiative forcing are not expected to sum to the total CO₂ response (Fig. 4a–d). For example, elevated CO₂ radiative forcing alone may be great enough to result in 100 additional summer heat wave days (out of 120 total summer days) in a particular location, while CO₂ vegetation forcing alone may cause sufficient warming to result in 40 more summer heat wave days in that same location.

The increases in summer heat wave days from CO₂ vegetation forcing are driven by more frequent and longer heat wave events (Fig. 4b, c, and Supplementary Figs. 6m–r and 7a–f). CO₂ vegetation forcing yields two to three more heat wave events per summer over the eastern US and eastern Europe, and over most of Canada and Asia. Tropical regions, including northwest South

America, equatorial Africa, and the Maritime Continent experience three to five more heat wave events per summer. While significant and notable, the vegetation effect on heat wave days and length is smaller than the effect of CO₂ radiative forcing alone (Supplementary Figs. 6g–l and 7g–l). The radiative response alone, for example, is sufficient to shift tropical and subtropical temperatures so far outside the range of natural variability that nearly all days in a climate with elevated CO₂ radiative forcing meet the heat wave day criteria, leading to long heat waves and fewer individual summer heat wave events in the tropics and subtropics in some models (Supplementary Fig. 6s–x).

CO₂ vegetation forcing increases the average length of the maximum summer heat wave event by more than eight days over the Amazon, Congo Basin, and Maritime Continent, and by as many as four to six days over much of the Northern Hemisphere mid-to-high latitudes (Fig. 4c). Heat wave intensity increases between 1 °C and 2 °C over portions of Canada, Europe, and Russia (Fig. 4d and Supplementary Fig. 7m–r). Smaller increases of 0.25 °C–1.5 °C are located in northwest South America, equatorial Africa, and the Maritime Continent. In several models, the increase in mid-to-high latitude heat wave intensity from CO₂ vegetation forcing is of similar magnitude to that from CO₂ radiative forcing (Fig. 4f and Supplementary Fig. 7m–x).

The simulated changes in heat wave metrics from CO₂ vegetation and CO₂ radiative forcing are robust to the choice of the reference climate (see Methods). The impacts of elevated end-of-21st-century CO₂ vegetation forcing and CO₂ radiative forcing within a historical period reference climate (relatively low CO₂) are very similar to those within a future reference climate (relatively high CO₂, see Supplementary Fig. 8). However, small differences in the changes in heat wave metrics from CO₂ vegetation forcing are present at high latitudes, where the choice of reference climate (low versus high CO₂) likely has a large impact on summer vegetation growth (compare Fig. 4a–d with Supplementary Fig. 8a–d). Not surprisingly, changes in heat wave metrics from projected mid-21st century CO₂ vegetation forcing (average CO₂ ~575 ppm, see Supplementary Fig. 8i–l) are smaller than those from the projected end of 21st century forcing (average

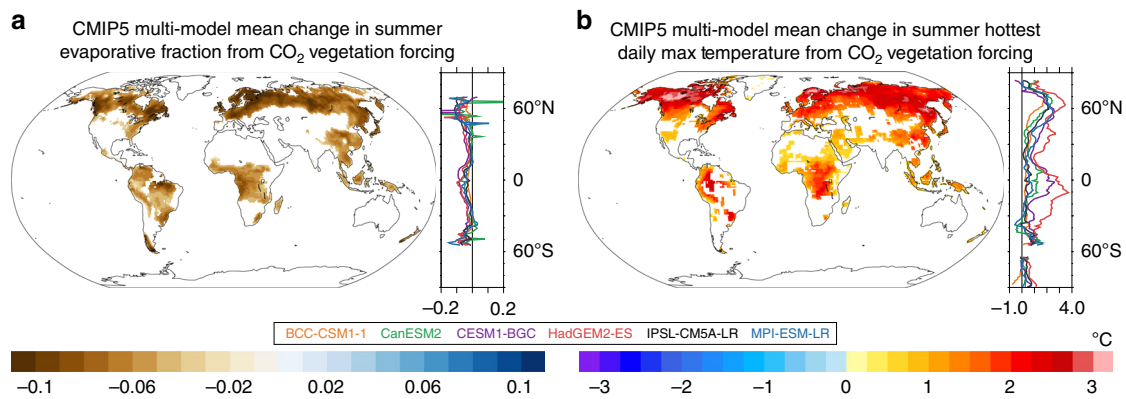


Fig. 3 Change in the evaporative fraction and surface temperature from CO₂ vegetation forcing. Multi-model mean change in summer **a** mean evaporative fraction (EF) (ratio of latent heat fluxes to the sum of sensible and latent heat fluxes), and **b** mean hottest daily maximum 2-meter temperature from CO₂ vegetation forcing. Only statistically significant changes are plotted (Methods). Zonal averages of EF change and hottest daily maximum temperature change (land grid points) for each model are plotted to the right of each map. Note, the magnitudes of EF change north of 65°N and over Antarctica are very large in some models, and are masked out in the zonal average plot. June–September (December–March) values are used in the Northern (Southern) Hemisphere. Plots represent 30-year averages

CO₂ ~984 ppm, see Fig. 4a–d), though the spatial patterns of extreme heat change (where statistically significant) are similar. Overall, the six CMIP5 models analyzed in this study suggest that projected CO₂ vegetation forcing will increase both the mean and upper tail (heat extremes) of the summer daily temperature distribution in most vegetated regions of the tropics and mid-to-high latitudes, enhancing the risk of acute impacts associated with heat wave events.

Growing season influence on summer season hydrology. To assess whether hydrologic and vegetation changes outside of the summer season shape the vegetation and climate response to elevated CO₂ during the summer, we explored the temporal relationship between surface hydrology, LAI, and heat waves in four regions with robust summer season heat wave changes: northeastern North America, Europe, tropical South America, and tropical Africa (Fig. 5 and Supplementary Fig. 9). In the mid-latitude locations, reduced springtime transpiration from CO₂ vegetation forcing contributes to slightly greater total-column soil moisture at the start of the summer season in most models (Fig. 5a, b and Supplementary Fig. 9a–l, see Supplementary Table 1 for the hydrologically active soil column depths in each model). However, reductions in spring precipitation from CO₂ vegetation forcing (with the exception of BCC-CSM1-1 in North America) limit the accumulation of soil moisture entering the summer season. Though this excess soil moisture is available to some plants during the summer, it does not increase summer transpiration. Rather, the transpiration response to CO₂ vegetation forcing remains negative during the summer months, leading to further increases in soil moisture. Soil moisture accumulation during the summer is limited by reduced summer precipitation. The reduction in summer precipitation from CO₂ vegetation forcing, which manifests in fewer summer rainfall days³⁵, enhances the likelihood of conditions favorable for heat wave development. Changes in surface evaporation (canopy plus soil) are small and contribute little to the surface water and heat flux changes from CO₂ vegetation forcing during the year.

In the evergreen tropics, CO₂ fertilization and CO₂ physiological forcing impact climate throughout the year (Fig. 5c, d and Supplementary Fig. 9m–x). Similar to the mid-latitude locations, CO₂ vegetation forcing reduces austral summer transpiration in the Congo and Amazon basins regardless of elevated summer LAI and greater soil moisture at the start of the summer season. It is worth noting that the small change in austral summer

transpiration and the large decrease in soil moisture in the Amazon in CanESM2 are the result of a substantial negative LAI bias (Supplementary Fig. 1), which diminishes the negative transpiration response in the multi-model mean plot (Fig. 5c). Additionally, the lack of austral summer transpiration decline in the Amazon in IPSL-CM5A is driven by a near 100% increase in LAI, a response not found in the other models (Supplementary Figs. 3e and 9q). Interestingly, most models do not exhibit a reduction in Amazon and Congo basin transpiration during the austral winter dry season (JJAS), when temperatures are at their climatological peak (Supplementary Figs. 9m–x). At the start of the dry season most models exhibit excess soil moisture from CO₂ vegetation forcing as a result of reduced austral spring-to-fall transpiration and, in some models, by increased summer-to-fall precipitation. The combination of excess soil moisture at the start of the dry season, greater LAI during the dry season, deep roots, and high evaporative demand are likely responsible for maintaining the same transpiration during this time (Fig. 5c) (e.g., ref. [12]). However, in most regions and times of the year, transpiration reductions in response to future CO₂ vegetation forcing in CMIP5 ESMs directly and indirectly (climate system feedbacks) lead to warmer temperatures and increased heat extremes regardless of soil moisture savings in previous months.

Discussion

Elevated CO₂ concentrations are expected to drive widespread increases in extreme heat events this century⁴¹. Most often, projections of future heat wave changes are attributed to the radiative impacts of higher CO₂. Here, we find that even without consideration of the radiative effects of CO₂, heat wave frequency will increase in vegetated regions as a consequence of vegetation's direct response to rising atmospheric CO₂ concentrations. Despite greater LAI from higher CO₂, reductions in stomatal conductance from CO₂ physiological forcing reduce warm season transpiration, limiting surface evaporative cooling, thus shifting both summer mean and extreme temperatures upward.

The greatest reductions in summer transpiration and subsequent increases in summer heat wave frequency, duration, and magnitude are located in tropical and mid-to-high latitude regions with dense tree cover and high climatological transpiration (Figs 1h, 4). These are regions in which transpiration is not strongly limited by water availability during much of the summer. The only areas where summer transpiration consistently increases in response to the combined influences of CO₂ physiological

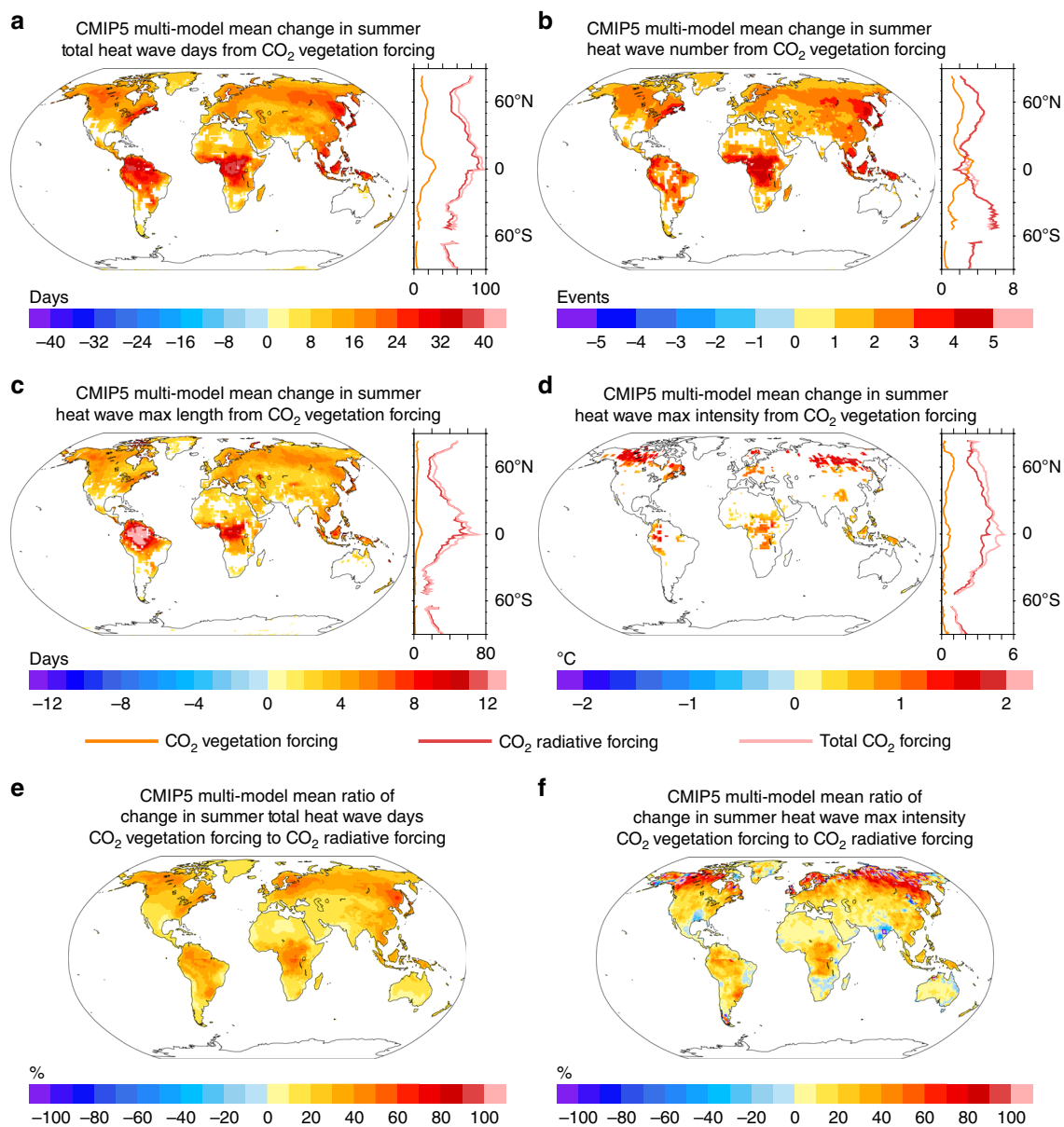


Fig. 4 Change in heat wave metrics from CO₂ vegetation forcing. Multi-model mean change in summer **a** total heat wave days (HWTD), **b** heat wave number (HWN), **c** heat wave maximum length (HWML), and **d** heat wave maximum intensity (HWMI) from CO₂ vegetation forcing (maps). Multi-model mean zonal averages of the change in each heat wave metric from (orange) CO₂ vegetation forcing, (red) CO₂ radiative forcing, and (pink) total CO₂ forcing. Only land grid points are used in the zonal averages. Multi-model mean ratio (percentage) of the change in **e** HWTD and **f** HWMI from CO₂ vegetation and CO₂ radiative forcing ($[\text{CO}_2 \text{ vegetation} / \text{CO}_2 \text{ radiative}] \times 100$). Only statistically significant changes are plotted in **a-d** (Methods). June–September (December–March) values are used in the Northern (Southern) Hemisphere. Plots represent 30-year averages

forcing and CO₂ fertilization are those located in warm, semi-arid, and arid climates (Fig. 2a, and Supplementary Figs. 2s–x and 3a–f). In these areas, models project substantial positive percent changes in LAI from CO₂ fertilization that counteract the impact of reduced stomatal conductance from CO₂ physiological forcing on transpiration (Supplementary Fig. 3a–f). These model projections are consistent with gas exchange theory and recent satellite observations that show the greatest impact of CO₂ fertilization in warm, arid climates where water is the dominant limiting factor for growth²³.

The CMIP5 results do not support the hypothesis that CO₂-vegetation forcing will reduce future mid-latitude summer heat waves¹². This hypothesis posits that reductions in spring transpiration from CO₂ physiological forcing increase the summer soil moisture available to cool surface temperatures. We find that

CO₂ vegetation forcing does increase spring season soil moisture in some regions in several of the CMIP5 ESMs (Fig. 5 and Supplementary Fig. 9). However, in the warm and arid regions where summer transpiration does increase slightly, the models do not project statistically significant reductions in summer heat waves (Fig. 4 and Supplementary Figs. 6–7). In most areas, the potential increase in transpiration from greater soil moisture and greater LAI does not balance the larger transpiration reduction induced by lower summer stomatal conductance, resulting in net decreases in summer transpiration and greater heat wave day frequency. In the presence of high CO₂, reduced stomatal conductance and transpiration appears to control soil moisture content in the CMIP5 models, rather than vice versa. The degree to which soil moisture influences model transpiration, often through a soil moisture stress parameter, is clearly important for

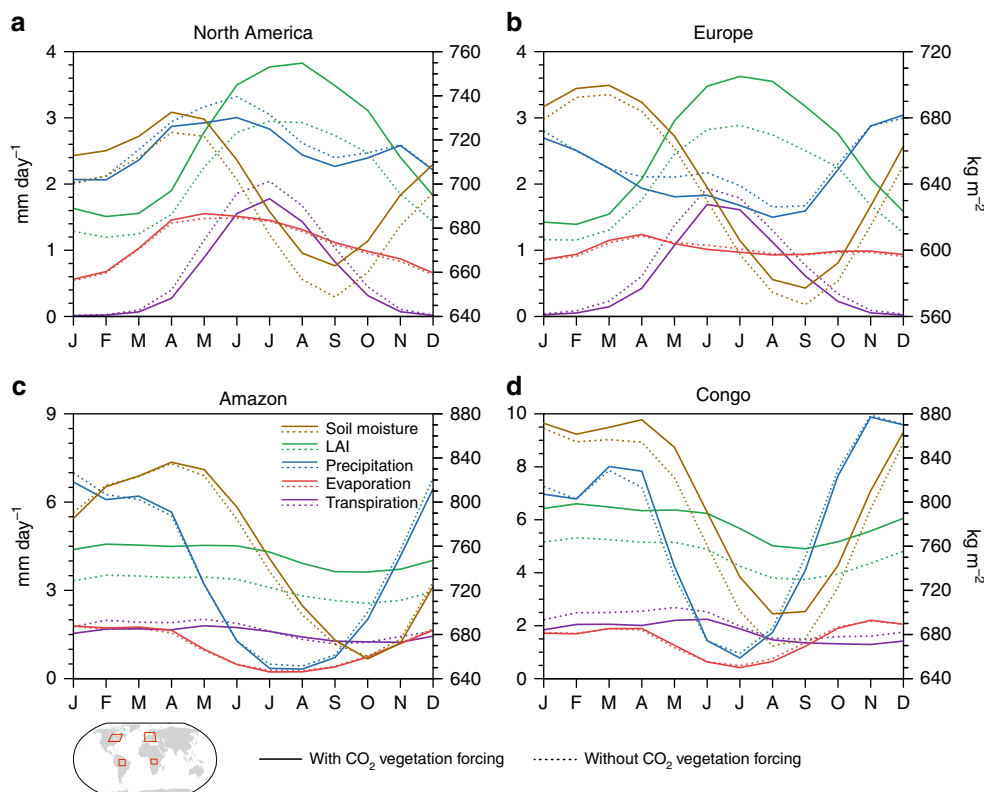


Fig. 5 Annual cycle of vegetation and hydrologic variables in simulations with and without future CO₂ vegetation forcing. CMIP5 multi-model mean area-weighted averages of total-column soil moisture (brown), leaf area index (LAI) (green), precipitation (blue), evaporation (red), and transpiration (purple) for portions of **a** North America (40°N–55°N, 100°W–70°W), **b** Europe (40°N–60°N, 0°–30°E), **c** the Amazon basin (0°–15°S, 65°W–50°W), and **d** the Congo basin (0°–10°S, 15°E–30°E). Dashed (solid) lines represent the final 30 years of the *RadCO2 (TotalCO2)* simulation. LAI (unitless), precipitation, evaporation, and transpiration correspond to the left y-axis. Soil moisture corresponds to the right y-axis. Output from HadGEM2-ES is not included in the plots

future projections of surface hydrology and extreme heat, and should be a focus of future land model development^{38,41}.

Reduced transpiration from CO₂ physiological forcing also initiates a number of climate system feedbacks that further enhance the likelihood and intensity of extreme heat events. In many mid and high latitude locations, a shift from latent to sensible heating (Fig. 3a) dries and stabilizes the boundary layer through lower ET and enhanced planetary boundary layer heights⁴². These regions experience fewer clouds, less rainfall, and greater surface solar insolation (Fig. 5a, b and Supplementary Fig. 4m–x). These changes lead to faster heat wave onset, enhanced heat wave temperatures, and longer heat wave events (Fig. 4). Future studies with access to daily-scale transpiration, winds, and geopotential heights should assess whether CO₂ vegetation forcing also alters the characteristics of atmospheric patterns that promote heat wave events.

Previous work that suggests CO₂ vegetation forcing will mitigate future mid-latitude heat waves utilizes a one-way nested regional climate model, which cannot capture these key climate system feedbacks¹². Indeed, the regional climate model study uses the same land surface model (ORCHIDEE)⁴³ as the one employed in the IPSL-CM5A-LR model from CMIP5, which exhibits some of the largest transpiration reductions coupled with heat wave increases in response to CO₂ vegetation forcing in the mid and high latitudes due to such feedbacks. As demonstrated with the global ESMs in this study, when assessing the potential impact of CO₂ vegetation forcing on future heat wave events, it is necessary to consider locally and remotely driven climate system feedbacks, including cloud and precipitation changes, which may contribute to the climate response. It is also important to note

that the regional climate modeling work in ref.¹² analyzed a particularly long and severe heat wave event (the European summer 2003 heat wave). While it is clear that CO₂ vegetation forcing enhances the intensity and frequency of future heat wave events within CMIP5 models in general, it is possible that CO₂ vegetation forcing may result in greater surface latent cooling and reduced temperatures during one of these anomalously long heat waves. ESMs from CMIP5 tend to underestimate the frequency of the most severe heat waves⁴⁴, and therefore may not be suited to fully assess the impact of CO₂ vegetation forcing on all types of heat wave events.

Consideration of the vegetation response to rising CO₂ helps to explain the spatial patterns and intermodel differences of projected future heat extremes. Across the subset of CMIP5 models analyzed in this study, those that most severely underestimate the annual ratio of transpiration to ET in the present-day also project the smallest changes in transpiration in response to CO₂ vegetation forcing (Fig. 2b). The models with the largest transpiration reductions from CO₂ vegetation forcing project the greatest increases in summer warming and heat wave days (Supplementary Figs. 2s–x, 5, and 6a–f). These results point to the important role of existing vegetation parameterizations in shaping projections of extreme heat events. Data-model intercomparisons, such as the Free-Air CO₂ Enrichment (FACE) Model-Data Synthesis project⁴¹ have identified a number of key processes responsible for model divergence in the simulation of transpiration, including the impact of soil moisture availability on stomatal conductance, the coupling between transpiration and canopy conductance, and the role of nutrient limitations. Though all models analyzed in this study project transpiration reductions and subsequent heat

wave increases due to CO₂ vegetation forcing, refinement of these model processes may help to constrain uncertainties in future heat wave projections. It is also important to note that several models from the larger CMIP5 ensemble (none of which are analyzed in this study) do not include the physiological effects of CO₂, as stomatal conductance in those models does not depend on CO₂⁴⁵. Our results suggest that projections from those models would underestimate future changes in extreme heat. Ensuring that all models include the dependence of stomatal conductance on CO₂ concentration may help to constrain future changes in heat extremes.

More broadly, the substantial role of vegetation physiology in shaping future simulated hydrology and surface energy fluxes in ESMs highlights the need to develop mechanistic models of plant growth and physiology and to increase observational efforts toward understanding vegetation's role in the hydrologic cycle. Presently, models use semi-empirical formulations of stomatal conductance that do not capture the full range of stomatal behavior across plants (e.g., ref.[31]). Similarly, models struggle to simulate observed relationships between elevated CO₂ and changes in LAI²⁷. Both of these factors limit confidence in projections of regional climate change, such as those presented in this study, and point to the need for increased process-based understanding and mechanistic models of stomatal conductance and carbon allocation in ESMs^{46,47}.

In terms of observations, the measurements of transpiration at large spatial scales are difficult to attain, and despite recent insights from stable isotope techniques⁴⁸ and satellite retrievals of LAI³⁹, estimates remain uncertain, making model-observation comparisons challenging. Additionally, a lack of FACE experiments in the tropics and high latitudes limits the ability to evaluate the modeled response of vegetation to elevated CO₂ in these regions. Future expansion of FACE experiments across biomes⁴⁹ will provide necessary validation of the large transpiration changes projected for the tropics and high latitudes (Fig. 1h and Supplementary Figure 2s-x). Model-data comparisons such as the FACE Model-Data Synthesis Project, which compare FACE data with output from land models forced with observed atmospheric conditions consistent with the FACE locations are a promising way forward for model evaluation⁴¹.

The CMIP5 experiments analyzed in this study suggest transpiration plays an important role in diminishing extreme heat events in the present climate. In a high-CO₂ world, model reductions in transpiration from CO₂ physiological forcing outpace potential increases in transpiration from CO₂ fertilization leading to widespread heat wave increases. Although temperatures and heat extremes will continue to increase after anthropogenic CO₂ emissions cease due to thermal inertia in the oceans⁵⁰, the results here suggest the stabilization of atmospheric CO₂ concentrations will have the immediate benefit of limiting further reductions in transpiration from CO₂ physiological forcing, mitigating vegetation's role in enhancing extreme heat events. Given the potential for vegetation changes to shape future surface energy and water fluxes, improved process-based understanding and model representation of the role of vegetation in the carbon and hydrologic cycles is needed to prepare for and mitigate the acute impacts of future heat extremes.

Methods

Model data and experimental design. We analyze simulations from six ESMs archived as part of the carbon-climate feedback experiment within CMIP5 (Table 1, Supplementary Table 1)⁵¹. The six ESMs are BCC-CSM1-1⁵², CanESM2⁵³, CESM1-BGC⁵⁴, IPSL-CM5A-LR⁵⁵, HadGEM2-ES⁵⁶, and MPI-ESM-LR⁵⁷, and are chosen based on the availability of daily-scale temperature data needed for the analysis of heat extremes. For each model we assess the impact of CO₂ vegetation forcing on climate by comparing two simulations: one simulation that includes the fully-interactive radiative, physiological, and fertilization effects of

increasing CO₂ (*TotalCO2*, denoted *1pctCO2* in CMIP5, see Table 1) and one simulation that includes only the radiative effects of increasing CO₂ (*RadCO2*, denoted *esmFdbk1* in CMIP5, see Table 1). For our purposes, the only difference between the two sets of simulations is whether the vegetation in the model is directly influenced by the increasing CO₂—in *RadCO2* it is not. Additionally, we assess the impact of CO₂ radiative forcing on climate by comparing the set of *TotalCO2* simulations to a set of simulations that includes only the physiological and fertilization effects of elevated CO₂ (*VegCO2*, see Table 1), (denoted *esmFix-Clim1* in CMIP5). For our purposes, the only difference between the two sets of simulations is whether the atmospheric radiative transfer scheme is directly influenced by the increasing CO₂—in *VegCO2* it is not. In all three sets of simulations, CO₂ concentrations increase by 1% per year for 140 years, starting at 284 ppm and ending at about 1132 ppm. For reference, CO₂ concentrations in the high emissions RCP8.5 scenario are roughly 935 ppm in the year 2100⁵⁹. Concentrations of aerosols and non-CO₂ greenhouse gases (other than water vapor) are fixed at preindustrial levels throughout each of the three 140-year simulations.

Our principal focus is on quantifying the impact of end-of-21st-century CO₂ vegetation forcing on heat waves relative to end-of-21st-century CO₂ radiative forcing. We calculate the impact of end-of-21st-century CO₂ vegetation forcing on climate by subtracting the final 30 years of data in *RadCO2* (end-of-21st-century radiative CO₂ forcing) from the final 30 years of data in *TotalCO2* (end-of-21st-century total CO₂ forcing, see Table 2). Likewise, we calculate the impact of end-of-21st-century CO₂ radiative forcing on climate by subtracting the final 30 years of data in *VegCO2* (end-of-21st-century vegetation CO₂ forcing) from the final 30 years of data in *TotalCO2* (end-of-21st-century total CO₂ forcing, see Table 2). We choose to analyze the final 30 years of each simulation (average CO₂ concentrations ~984 ppm) in order to assess modeled CO₂ vegetation forcing and CO₂ radiative forcing that are generally consistent with a high emissions scenario projection (RCP8.5) for the end of the 21st century⁵⁸.

We emphasize that we use the *RadCO2* simulations to back out the influence of CO₂ vegetation forcing on climate (i.e., *TotalCO2* – *RadCO2*) rather than using the *VegCO2* simulations directly (and vice versa for CO₂ radiative forcing) because it allows for an assessment of CO₂ vegetation forcing (CO₂ radiative forcing) relative to future CO₂ radiative forcing (CO₂ vegetation forcing).

Our focus is on the summer season in each hemisphere (June–September (JJAS), in the Northern Hemisphere, December–March (DJFM) in the Southern Hemisphere), when mean temperatures and heat extremes reach their maximum intensity. We use the permutation test to assess the statistical significance of the differences between the simulations at the 95% confidence level within each individual model, and present multi-model mean figures to show model agreement. Within the multi-model mean figures, a grid box is filled with the mean value of all six ESMs when at least four of the six models exhibit statistically significant changes in the same direction as the multi-model mean change at that grid point. When a location does not meet these criteria, the grid box is left unfilled (white). Maps for each individual model are provided as Supplementary Figures. The HadGEM2-ES model does not archive evaporation or transpiration variables and is therefore not included in the multi-model mean plots for those variables; we explicitly noted this when we use HadGEM2-ES ET as a fill-in for evaporation or transpiration.

Heat wave detection. Heat waves are detected following⁵⁹ and the indices for monitoring temperature extremes put forth by the World Meteorological Organization (WMO) Commission for Climatology (CCI)/Climate Variability and Predictability (CLIVAR)/Joint Technical Commission for Oceanography and Marine Meteorology (JCOMM) Expert Team on Climate Change Detection and Indices (ETCCDI)⁶⁰. Specifically, a heat wave is defined as an event of at least three consecutive days during which the daily maximum temperature exceeds the calendar day 90th percentile value from a reference period, based on a 5-day moving average. A percentile value for each calendar day is used to account for seasonality, and a 5-day moving average is used to account for temporal autocorrelation in the daily data⁵⁹.

We used four heat wave metrics to characterize changes in extreme heat events: The HWTD is the sum of all days that meet the heat wave criteria each season. The heat wave maximum length (HWML) is the length in days of the longest heat wave event each season. The heat wave number (HWN) is the average number of heat waves per season. The heat wave maximum intensity (HWMI) is the maximum daily temperature reached during each heat wave event during the season. All metrics are calculated for each year and then averaged over the 30-year time period.

The reference period used to calculate temperature percentiles and heat waves depends on the CO₂ forcing of interest. Given our experimental design (see above), the reference period for calculating changes in heat waves due to end-of-21st-century CO₂ vegetation forcing is the final 30 years of *RadCO2*. The reference period for calculating changes in heat waves due to end-of-21st-century CO₂ radiative forcing is the final 30 years of *VegCO2*.

Sensitivity analyses. We provide two sensitivity analyses for our results. First, to assess the influence of our chosen reference climate on changes in heat extremes, we also analyze the change in heat wave indices within (rather than across) model simulations by subtracting the first 30 years of data in the *VegCO2* (*RadCO2*)

simulation from the final 30 years of data in the *VegCO2* (*RadCO2*) simulation (Table 2). We also quantify the total CO₂-driven (CO₂ vegetation forcing + CO₂ radiative forcing) response of heat extremes by subtracting the first 30 years of the *TotalCO2* simulation from the final 30 years of the *TotalCO2* simulation. Accordingly, in these analyses, the reference period temperature thresholds and heat waves are defined using the first 30 years of data in *VegCO2*, *RadCO2*, and *TotalCO2*.

Second, to assess the influence of different levels of CO₂-forcing on our results, we also analyze the vegetation-driven responses of extreme heat metrics for CO₂ concentrations consistent with the middle 21st century in a high emissions scenario (~575 ppm). To assess the impact of mid-century CO₂ vegetation forcing we subtract the 30-year time period between years 58 and 87 of the *RadCO2* simulation from the corresponding 30-year time period in the *TotalCO2* simulation (Table 2). Simulation years 58–87 are chosen to reflect CO₂ values that are roughly consistent with years 2040–2070 in the RCP8.5 pathway⁵⁸.

Model vegetation description and validation. CO₂ physiological forcing is directly tied to the representation and response of stomatal conductance in the models. All six ESMs relate stomatal conductance to photosynthesis via semi-empirical formulations. Five of the six ESMs use either the Ball–Berry conductance model⁶¹ or the Leuning conductance model⁶² (Supplementary Table 1). The primary difference between the two formulations is their treatment of atmospheric moisture content: Ball–Berry uses relative humidity while Leuning uses vapor pressure deficit. In the sixth model, MPI-ESM-LR, the formulation of stomatal conductance does not include a dependency on atmospheric humidity^{63,64}. All else equal, all models exhibit reductions in stomatal conductance in response to elevated atmospheric CO₂ concentrations at the leaf surface based on their functional forms.

Calculations of LAI are prognostic in all ESMs and depend on plant carbon stocks (in part determined by CO₂ fertilization), carbon allocation (the distribution of carbon to leaves, roots, and stems), and leaf turnover rates, as well as climate factors including temperature, soil moisture, and sunlight³⁷. HadGEM2-ES and MPI-ESM-LR both include dynamic vegetation modules (Supplementary Table 1), which allow the communal assemblages of plant functional types to change, though inclusion of dynamic biogeography appears to have little effect on intermodel differences in projected LAIs³⁷. We compare ESM simulations of LAI with the satellite-based AVH15C1 LAI dataset (years spanning 1980–2010) derived from the National Oceanic and Atmospheric Administration (NOAA) Climate Data Record (CDR) of Advanced Very High Resolution Radiometer (AVHRR) Surface Reflectance⁶⁵.

All data (observations and CMIP5) are interpolated to a common 1° × 1° grid using a patch recovery method⁶⁶.

Data availability. All CMIP5 data analyzed in the current study are publicly available on the Earth System Grid Federation website: <https://esgf.llnl.gov/>. Observed LAI data from the NOAA CDR of AVHRR Surface Reflectance are publicly available from the NOAA National Centers for Environmental Information (NCEI) website:

<https://data.nodc.noaa.gov/cgi-bin/iso?id=gov.noaa.ncdc:C00898>

Received: 21 July 2017 Accepted: 15 February 2018

Published online: 15 March 2018

References

- Semenza, J. C. et al. Heat-related deaths during the July 1995 heat wave in Chicago. *New Engl. J. Med.* **335**, 84–90 (1996).
- Fouillet, A. et al. Excess mortality related to the August 2003 heat wave in France. *Int. Arch. Occup. Environ. Health* **80**, 16–24 (2006).
- García-Herrera, R., Díaz, J., Trigo, R. M., Luterbacher, J. & Fischer, E. M. A review of the European summer heat wave of 2003. *Crit. Rev. Environ. Sci. Technol.* **40**, 267–306 (2010).
- Gouveia, C. M. et al. The outstanding synergy between drought, heatwaves and fuel on the 2007 Southern Greece exceptional fire season. *Agric. For. Meteorol.* **218–219**, 135–145 (2016).
- Ciais, P. et al. Europe-wide reduction in primary productivity caused by the heat and drought in 2003. *Nature* **437**, 529–533 (2005).
- Horton, R. M., Mankin, J. S., Lesk, C., Coffel, E. & Raymond, C. A review of recent advances in research on extreme heat events. *Curr. Clim. Change Rep.* **2**, 242–259 (2016).
- Horton, D. E. et al. Contribution of changes in atmospheric circulation patterns to extreme temperature trends. *Nature* **522**, 465–469 (2015).
- Meehl, G. A. & Tebaldi, C. More intense, more frequent, and longer lasting heat waves in the 21st Century. *Science* **305**, 994 (2004).
- Fischer, E. M. & Schar, C. Consistent geographical patterns of changes in high-impact European heatwaves. *Nat. Geosci.* **3**, 398–403 (2010).
- Petoukhov, V., Rahmstorf, S., Petri, S. & Schellnhuber, H. J. Quasiresonant amplification of planetary waves and recent Northern Hemisphere weather extremes. *Proc. Natl Acad. Sci. USA* **110**, 5336–5341 (2013).
- Kala, J. et al. Impact of the representation of stomatal conductance on model projections of heatwave intensity. *Sci. Rep.* **6**, 23418 (2016).
- Lemordant, L., Gentine, P., Stefanon, M., Drobinski, P. & Faticchi, S. Modification of land-atmosphere interactions by CO₂ effects: implications for summer dryness and heat wave amplitude. *Geophys. Res. Lett.* **43**, 240–210,248 (2016).
- Taylor, K. E., Stouffer, R. J. & Meehl, G. A. An overview of CMIP5 and the experiment design. *Bull. Am. Meteorol. Soc.* **93**, 485–498 (2011).
- Ainsworth, E. A. & Rogers, A. The response of photosynthesis and stomatal conductance to rising [CO₂]: mechanisms and environmental interactions. *Plant Cell. Environ.* **30**, 258–270 (2007).
- Cowling, S. A. & Field, C. B. Environmental control of leaf area production: implications for vegetation and land-surface modeling. *Glob. Biogeochem. Cycles* **17**, 7–1–7–14 (2003).
- Zhu, Z. et al. Greening of the Earth and its drivers. *Nat. Clim. Change* **6**, 791–795 (2016).
- Sellers, P. J. et al. A revised land surface parameterization (SiB2) for atmospheric GCMs. Part II: The generation of global fields of terrestrial biophysical parameters from satellite data. *J. Clim.* **9**, 706–737 (1996).
- Betts, R. A. et al. Projected increase in continental runoff due to plant responses to increasing carbon dioxide. *Nature* **448**, 1037–1041 (2007).
- Kergoat, L. Impact of doubled CO₂ on global-scale leaf area index and evapotranspiration: Conflicting stomatal conductance and LAI responses. *J. Geophys. Res.* **107**, 30–1–30–16 (2002).
- Ainsworth, E. A. & Long, S. P. What have we learned from 15 years of free-air CO₂ enrichment (FACE)? A meta-analytic review of the responses of photosynthesis, canopy properties and plant production to rising CO₂. *New Phytol.* **165**, 351–372 (2005).
- Norby, R. J. & Zak, D. R. Ecological lessons from free-air CO₂ enrichment (FACE) Experiments. *Annu. Rev. Ecol., Evol., Syst.* **42**, 181–203 (2011).
- Warren, J. M. et al. Ecohydrologic impact of reduced stomatal conductance in forests exposed to elevated CO₂. *Ecohydrology* **4**, 196–210 (2011).
- Donohue, R. J., Roderick, M. L., McVicar, T. R. & Farquhar, G. D. Impact of CO₂ fertilization on maximum foliage cover across the globe's warm, arid environments. *Geophys. Res. Lett.* **40**, 3031–3035 (2013).
- Field, C. B., Jackson, R. B. & Mooney, H. A. Stomatal responses to increased CO₂: implications from the plant to the global scale. *Plant Cell. Environ.* **18**, 1214–1225 (1995).
- Zeng, Z. et al. Climate mitigation from vegetation biophysical feedbacks during the past three decades. *Nat. Clim. Change* **7**, 432–436 (2017).
- Cao, L., Bala, G., Caldeira, K., Nemani, R. & Ban-Weiss, G. Importance of carbon dioxide physiological forcing to future climate change. *Proc. Natl Acad. Sci. USA* **107**, 9513–9518 (2010).
- Faticchi, S. et al. Partitioning direct and indirect effects reveals the response of water-limited ecosystems to elevated CO₂. *Proc. Natl Acad. Sci. USA* **113**, 12757–12762 (2016).
- Screen, J. A. & Simmonds, I. Amplified mid-latitude planetary waves favour particular regional weather extremes. *Nat. Clim. Change* **4**, 704–709 (2014).
- Hirschi, M. et al. Observational evidence for soil-moisture impact on hot extremes in southeastern Europe. *Nat. Geosci.* **4**, 17–21 (2011).
- Field, C., Lund, C., Chiariello, N. & Mortimer, B. CO₂ effects on the water budget of grassland microcosm communities. *Glob. Change Biol.* **3**, 197–206 (1997).
- Keel, S. G., Pepin, S., Leuzinger, S. & Körner, C. Stomatal conductance in mature deciduous forest trees exposed to elevated CO₂. *Trees* **21**, 151–159 (2007).
- Mueller, N. D. et al. Cooling of US Midwest summer temperature extremes from cropland intensification. *Nat. Clim. Change* **6**, 317–322 (2015).
- Thiery, W. et al. Present-day irrigation mitigates heat extremes. *J. Geophys. Res.: Atmospheres* **122**, 1403–1422 (2017).
- Swann, A. L. S., Hoffman, F. M., Koven, C. D. & Randerson, J. T. Plant responses to increasing CO₂ reduce estimates of climate impacts on drought severity. *Proc. Natl Acad. Sci. USA* **113**, 10019–10024 (2016).
- Skinner, C. B., Poulsen, C. J., Chadwick, R., Diffenbaugh, N. S. & Fiorella, R. P. The role of plant CO₂ physiological forcing in shaping future daily-scale precipitation. *J. Clim.* **30**, 2319–2340 (2017).
- Sillmann, J., Kharin, V. V., Zwiers, F. W., Zhang, X. & Bronaugh, D. Climate extremes indices in the CMIP5 multimodel ensemble: Part 2. Future climate projections. *J. Geophys. Res.: Atmospheres* **118**, 2473–2493 (2013).
- Mahowald, N. et al. Projections of leaf area index in earth system models. *Earth Syst. Dyn.* **7**, 211–229 (2016).
- Mankin, J. S., Smerdon, J. E., Cook, B. I., Williams, A. P. & Seager, R. The curious case of projected twenty-first-century drying but greening in the American west. *J. Clim.* **30**, 8689–8710 (2017).
- Wei, Z. et al. Revisiting the contribution of transpiration to global terrestrial evapotranspiration. *Geophys. Res. Lett.* **44**, 2792–2801 (2017).

40. Lombardozi, D. L., Zeppel, M. J. B., Fisher, R. A. & Tawfik, A. Representing nighttime and minimum conductance in CLM4.5: global hydrology and carbon sensitivity analysis using observational constraints. *Geosci. Model Dev.* **10**, 321–331 (2017).
41. De Kauwe, M. G. et al. Forest water use and water use efficiency at elevated CO₂: a model-data intercomparison at two contrasting temperate forest FACE sites. *Glob. Change Biol.* **19**, 1759–1779 (2013).
42. de Arellano, J. V.-G., van Heerwaarden, C. C. & Lelieveld, J. Modelled suppression of boundary-layer clouds by plants in a CO₂-rich atmosphere. *Nat. Geosci.* **5**, 701–704 (2012).
43. Krinner, G. et al. A dynamic global vegetation model for studies of the coupled atmosphere-biosphere system. *Glob. Biogeochem. Cycles* **19**, GB1015 (2005).
44. Russo, S. et al. Magnitude of extreme heat waves in present climate and their projection in a warming world. *J. Geophys. Res.: Atmospheres* **119**, 500–12,512 (2014).
45. DeAngelis, A. M., Qu, X. & Hall, A. Importance of vegetation processes for model spread in the fast precipitation response to CO₂ forcing. *Geophys. Res. Lett.* **43**, 550–12,559 (2016).
46. Ewert, F. Modelling plant responses to elevated CO₂: how important is leaf area index? *Ann. Bot. (Lond.)* **93**, 619–627 (2004).
47. Damour, G., Simonneau, T., Cochard, H. & Urban, L. An overview of models of stomatal conductance at the leaf level. *Plant Cell. Environ.* **33**, 1419–1438 (2010).
48. Good, S. P., Noone, D. & Bowen, G. Hydrologic connectivity constrains partitioning of global terrestrial water fluxes. *Science* **349**, 175–177 (2015).
49. Norby, R. J. et al. Model–data synthesis for the next generation of forest free-air CO₂ enrichment (FACE) experiments. *New Phytol.* **209**, 17–28 (2016).
50. Katharine, L. R. & Ken, C. Maximum warming occurs about one decade after a carbon dioxide emission. *Environ. Res. Lett.* **9**, 124002 (2014).
51. Arora, V. K. et al. Carbon–concentration and carbon–climate feedbacks in CMIP5 earth system models. *J. Clim.* **26**, 5289–5314 (2013).
52. Wu, T. et al. An overview of BCC climate system model development and application for climate change studies. *J. Meteorol. Res.* **28**, 34–56 (2014).
53. Arora, V. K. et al. Carbon emission limits required to satisfy future representative concentration pathways of greenhouse gases. *Geophys. Res. Lett.* **38**, L05805 (2011).
54. Lindsay, K. et al. Preindustrial-control and Twentieth-century Carbon cycle experiments with the earth system model CESM1(BGC). *J. Clim.* **27**, 8981–9005 (2014).
55. Dufresne, J. L. et al. Climate change projections using the IPSL-CM5 Earth System Model: from CMIP3 to CMIP5. *Clim. Dyn.* **40**, 2123–2165 (2013).
56. Jones, C. D. et al. The HadGEM2-ES implementation of CMIP5 centennial simulations. *Geosci. Model Dev.* **4**, 543–570 (2011).
57. Giorgetta, M. A. et al. Climate and carbon cycle changes from 1850 to 2100 in MPI-ESM simulations for the Coupled Model Intercomparison Project phase 5. *J. Adv. Model. Earth Syst.* **5**, 572–597 (2013).
58. Meinshausen, M. et al. The RCP greenhouse gas concentrations and their extensions from 1765 to 2300. *Clim. Change* **109**, 213–241 (2011).
59. Perkins, S. E. & Alexander, L. V. On the measurement of heat waves. *J. Clim.* **26**, 4500–4517 (2012).
60. Zhang, X. et al. Indices for monitoring changes in extremes based on daily temperature and precipitation data. *Wiley Interdiscip. Rev.: Clim. Change* **2**, 851–870 (2011).
61. Ball, J. T., Woodrow, I. E. & Berry, J. A. In *Progress in Photosynthesis Research*, Vol. 4. *Proceedings of the VIIth International Congress on Photosynthesis*. Providence, Rhode Island, USA, August 10–15, 1986 (ed. Biggins, J.) 221–224 (Springer, Netherlands, 1987).
62. Leuning, R. A critical appraisal of a combined stomatal-photosynthesis model for C₃ plants. *Plant Cell. Environ.* **18**, 339–355 (1995).
63. Knorr, W. Annual and interannual CO₂ exchanges of the terrestrial biosphere: process-based simulations and uncertainties. *Glob. Ecol. Biogeogr.* **9**, 225–252 (2000).
64. Knauer, J., Werner, C. & Zaehle, S. Evaluating stomatal models and their atmospheric drought response in a land surface scheme: a multibiome analysis. *J. Geophys. Res.: Biogeosciences* **120**, 1894–1911 (2015).
65. Claverie, M., Matthews, L. J., Vermote, F. E. & Justice, O. C. A 30+Year AVHRR LAI and FAPAR climate data record: algorithm description and validation. *Remote Sens.* **8**, 263–274 (2016).
66. Gu, H., Zong, Z. & Hung, K. C. A modified superconvergent patch recovery method and its application to large deformation problems. *Finite Elem. Anal. Des.* **40**, 665–687 (2004).

Acknowledgements

This work was supported by the Turner Postdoctoral Fellowship awarded to Christopher Skinner and by National Science Foundation Award 1602956. Justin S. Mankin was supported by The Earth Institute of Columbia University. We wish to thank Jürgen Knauer for helpful discussions. We acknowledge the World Climate Research Program and the climate modeling groups for making available their model output, and the U.S. Department of Energy's Program for Climate Model Diagnosis and Intercomparison for coordinating and supporting database development. This research was supported in part through computational resources and services provided by Advanced Research Computing at the University of Michigan, Ann Arbor. Lamont contribution number 8196.

Author contributions

C.B.S. conceived of the study and conducted the analysis. C.B.S., C.J.P., and J.S.M. interpreted the results and wrote the paper.

Additional information

Supplementary Information accompanies this paper at <https://doi.org/10.1038/s41467-018-03472-w>.

Competing interests: The authors declare no competing interests.

Reprints and permission information is available online at <http://npg.nature.com/reprintsandpermissions/>

Publisher's note: Springer Nature remains neutral with regard to jurisdictional claims in published maps and institutional affiliations.



Open Access This article is licensed under a Creative Commons Attribution 4.0 International License, which permits use, sharing,

adaptation, distribution and reproduction in any medium or format, as long as you give appropriate credit to the original author(s) and the source, provide a link to the Creative Commons license, and indicate if changes were made. The images or other third party material in this article are included in the article's Creative Commons license, unless indicated otherwise in a credit line to the material. If material is not included in the article's Creative Commons license and your intended use is not permitted by statutory regulation or exceeds the permitted use, you will need to obtain permission directly from the copyright holder. To view a copy of this license, visit <http://creativecommons.org/licenses/by/4.0/>.

© The Author(s) 2018